

# Investigation on Mechanical Behavior of I-Section Steel Columns After Elevated Temperature

Yu Chen\* , College of Civil Engineering, Fuzhou University, Fuzhou 350116, China; School of Urban Construction, Yangtze University, Jingzhou 434023, China

Wentao Xie, Shaohua Han and Kai Wang, School of Urban Construction, Yangtze University, Jingzhou 434023, China

**Received:** 14 October 2016/**Accepted:** 22 December 2017

**Abstract.** This paper presents the experimental and numerical investigations on mechanical behavior of I-section steel columns after elevated temperature exposure. A total of twenty-six compression tests were carried out, in which one was under ambient temperature and the other twenty-five were under heating and cooling phase to study the influence of high temperature (400, 550, 700, 850, 1000°C) and high temperature duration (0.5, 1, 1.5, 2, 2.5 h) on mechanical behavior of the specimens. The failure pattern, axial load versus strain relation, axial load versus displacement relation and ultimate strength of the specimens were presented and analyzed. The test results showed that, high temperature duration had limited influence on the ultimate strength and other mechanical behaviors of the specimens, while the ultimate strength decreases with the increase of the maximum temperature the specimens suffered and some other behaviors also changed. The failure pattern of specimens after high temperature did not change compared with that of specimens under ambient temperature. The finite element models that have the same geometry with the test specimens were set up to compare with the test specimens and the results predicted from finite element analysis showed good agreement with that measured in test. Therefore, parametric study was carried out to investigate the influence of different section geometry on the ultimate strength of I-section steel short columns after elevated temperature. A new relationship for the ultimate strength for I-section steel short columns after elevated temperature was developed and proved to be reliable and accurate. What's more, the effect of slenderness ratio on the stability coefficient of the columns was also investigated in the parametric study.

**Keywords:** I-section steel, Steel columns, High temperature, Fire temperature behaviour, Parametric study fire conditions

## List of symbols

|     |  |
|-----|--|
| $T$ | Maximum temperature the specimens suffered |
| $t$ | High temperature duration                  |
| $h$ | Section height of the specimens            |

---

\* Correspondence should be addressed to: Yu Chen, E-mail: [kinkinging@163.com](mailto:kinkinging@163.com)



|               |   |
|---------------|---|
| $b$           | Width of flange plate of the specimens                                |
| $d1$          | Thickness of web of the specimens                                     |
| $d2$          | Average thickness of flange plate of the specimens                    |
| $L$           | Height of the specimens   |
| $P$           | Axial load  |
| $\varepsilon$ | Strain of the specimens   |
| $\Delta$      | Displacement of the specimens   |
| $P_0$         | Ultimate strength of the specimen without high temperature exposure   |
| $P_u$         | Ultimate load of specimens after high temperature                     |
| $P_y$         | Yield load of specimens after high temperature                        |
| $k$           | Initial stiffness of the specimens                                    |
| $\Delta u$    | Displacement of the specimens corresponding to the ultimate load      |
| $\Delta y$    | Displacement of the specimens corresponding to the yield load         |
| $P1$          | Average ultimate strength of specimens at a certain temperature       |
| $\gamma$      | Load bearing capacity coefficient                                     |
| $f_y$         | Yield strength of the Q235 steel after high temperature               |
| $f_u$         | Ultimate strength of the Q235 steel after high temperature            |
| $\delta$      | Elongation of the Q235 steel after high temperature                   |
| $E$           | Elastic modulus of the Q235 steel after high temperature              |
| $\alpha$      | Height-to-thickness ratio of web of the finite element models         |
| $\beta$       | Width-to-thickness ratio of flange of the finite element models       |
| $h$           | Height of web of the finite element models                            |
| $b$           | Width of flange of the finite element models                          |
| $F_u$         | Calculated ultimate load  |
| $f_{y0}$      | Yield strength of the Q235 steel under room temperature               |
| $F_m$         | Ultimate strength obtained from the parametric study                  |
| COV           | Coefficient of variation  |
| $\Lambda$     | Slenderness ratio of the column                                       |
| $N_m$         | Load bearing capacity of the columns with different slenderness ratio |
| $\Psi$        | Stability coefficient   |
| $\psi_m$      | Stability coefficient obtained from FEA                               |
| $\psi_u$      | Stability coefficient obtained from the formula                       |

## 1. Introduction

I-section steel columns have been widely used in steel structures due to their unique advantages of simple production process, uniform texture, light weight, high strength, perfect ductility and toughness, however steel structures are poor in resistance of fire or high temperature.

In the past decades, mechanical behaviors of the steel column after fire or in fire have been extensively studied by different researchers. Tondini et al. [1] carried out a series of tests on samples of high-strength steel circular columns at elevated temperatures. Kervalishvili and Talvik [2] studied the stability of axially loaded steel columns with square hollow sections in fire and developed an alternative approach to calculate its buckling. Yang and Yang [3] used experimental methods to investigate the effect of the load ratios, weld details, and the width to thickness ratios on the fire behavior of welded steel box columns. Fan et al. [4] performed the fire test on eight square sections of stainless steel columns mainly to investigate the effects of the section dimension, load ratio, and eccentricity on the fire performance of the stainless steel column. The test results show that eccentricity and load ratio are the key factors for fire performance of the stainless steel col-

umn. Feng et al. [5] conducted an experimental study on 52 cold-formed thin-walled short steel channel columns at high temperatures to study the physical behavior and failure modes of this type of columns. Cheng et al. [6] presented a numerical investigation on the buckling behavior of channel-section columns. Scullion et al. [7] performed an experimental study on behavior of elliptical section steel columns in fire. Yang et al. [8] conducted a series of H steel columns under fire load. The tests results show that the slenderness ratios of steel columns and width-to-thickness ratio of steel plates are two key factors linked to global buckling of columns and local buckling, respectively. Yang and Hsu [9] conducted a series of experiments to examine the effect of the slenderness ratio of steel columns, the width-to-thickness ratio of flanges, and residual stresses on the ultimate strength of H steel column at elevated temperature. Ragheb [10] developed an inelastic stability model to investigate the local buckling performance of structural steel I-section columns at high temperatures. On the basis of this model, effects of several parameters on the local buckling capacity of steel I-section columns were also investigated. In order to study the effect of stiffness of the surrounding structure on steel I-section columns at elevated temperatures, Correia and Rodrigues [11] conducted a great many fire resistance tests. The results showed that the column's critical temperature did not reduce with increasing of the stiffness of the surrounding structure. It was also found that the higher initial load levels in fire resulted in shorter critical temperatures of the steel columns. All these researches as above are investigating the mechanical properties of steel column in fire. However, fire safety should not only consider the performance of the structure during the fire exposure but also the behavior after cooling. During fire disaster, steel structures are inevitably exposed to elevated temperatures; provided that structural collapse does not occur after fire events, the residual performance of such structures must be estimated accurately to determine whether they should be dismantled, repaired, or directly reused. Lu et al. [12] carried out a great many experiments on cold-formed Q235 steels as well as on hot-rolled Q235, Q345, and Q420 steels. During the process, specimens were heated to various elevated temperatures and cooled down to ambient temperature via two different methods, namely, air and water cooling. Tensile coupon tests were performed to obtain the post-fire stress-strain curves, ultimate strengths elastic moduli, ductility and yield strengths. Jin et al. [13] conducted both experimental and parametric study on the behavior of tubular T-joint after exposure to fire. The results show that the failure of a tubular T-joint was due to local buckling and it found the law of how the three parameters affect load-bearing capacity of the T-joint after fire.

At present, limited investigations about mechanical behavior of I-section steel columns after high temperature have been conducted. The tests and numerical simulations presented in this paper were developed to understand the residual performance of I-section steel columns after exposed to elevated temperatures.

## 2. Experimental Study

### 2.1. Specimens Preparations

The residual mechanical behaviors of 26 I-section steel short columns after high temperature were experimentally studied while subjected to axial compression. The main variables in the tests include:

- Maximum temperature ( $T$ ): 20, 400, 550, 700, 850 and 1000°C
- High temperature duration ( $t$ ): 0.5, 1.0, 1.5, 2.0 and 2.5 h

All specimens have the same geometry, a summary of the test information is presented in Table 1, where  $h$  is the section height of the specimens;  $b$  is the width of flange;  $d1$  is the thickness of web;  $d2$  is the average thickness of flange plate;  $L$  is the height of the specimens. All the cross sections of the columns in experiment were classified as class 1 according to Eurocode3.

**Table 1**  
**Details of Specimens in Test**

| Label      | $h$ (mm) | $b$ (mm) | $d1$ (mm) | $d2$ (mm) | $L$ (mm) | $T$ (°C) | $t$ (h) |
|------------|----------|----------|-----------|-----------|----------|----------|---------|
| IT20t0     | 100      | 68       | 4.5       | 7.6       | 200      | 20       | 0.0     |
| IT400t0.5  | 100      | 68       | 4.5       | 7.6       | 200      | 400      | 0.5     |
| IT400t1.0  | 100      | 68       | 4.5       | 7.6       | 200      | 400      | 1.0     |
| IT400t1.5  | 100      | 68       | 4.5       | 7.6       | 200      | 400      | 1.5     |
| IT400t2.0  | 100      | 68       | 4.5       | 7.6       | 200      | 400      | 2.0     |
| IT400t2.5  | 100      | 68       | 4.5       | 7.6       | 200      | 400      | 2.5     |
| IT550t0.5  | 100      | 68       | 4.5       | 7.6       | 200      | 550      | 0.5     |
| IT550t1.0  | 100      | 68       | 4.5       | 7.6       | 200      | 550      | 1.0     |
| IT550t1.5  | 100      | 68       | 4.5       | 7.6       | 200      | 550      | 1.5     |
| IT550t2.0  | 100      | 68       | 4.5       | 7.6       | 200      | 550      | 2.0     |
| IT550t2.5  | 100      | 68       | 4.5       | 7.6       | 200      | 550      | 2.5     |
| IT700t0.5  | 100      | 68       | 4.5       | 7.6       | 200      | 700      | 0.5     |
| IT700t1.0  | 100      | 68       | 4.5       | 7.6       | 200      | 700      | 1.0     |
| IT700t1.5  | 100      | 68       | 4.5       | 7.6       | 200      | 700      | 1.5     |
| IT700t2.0  | 100      | 68       | 4.5       | 7.6       | 200      | 700      | 2.0     |
| IT700t2.5  | 100      | 68       | 4.5       | 7.6       | 200      | 700      | 2.5     |
| IT850t0.5  | 100      | 68       | 4.5       | 7.6       | 200      | 850      | 0.5     |
| IT850t1.0  | 100      | 68       | 4.5       | 7.6       | 200      | 850      | 1.0     |
| IT850t1.5  | 100      | 68       | 4.5       | 7.6       | 200      | 850      | 1.5     |
| IT850t2.0  | 100      | 68       | 4.5       | 7.6       | 200      | 850      | 2.0     |
| IT850t2.5  | 100      | 68       | 4.5       | 7.6       | 200      | 850      | 2.5     |
| IT1000t0.5 | 100      | 68       | 4.5       | 7.6       | 200      | 1000     | 0.5     |
| IT1000t1.0 | 100      | 68       | 4.5       | 7.6       | 200      | 1000     | 1.0     |
| IT1000t1.5 | 100      | 68       | 4.5       | 7.6       | 200      | 1000     | 1.5     |
| IT1000t2.0 | 100      | 68       | 4.5       | 7.6       | 200      | 1000     | 2.0     |
| IT1000t2.5 | 100      | 68       | 4.5       | 7.6       | 200      | 1000     | 2.5     |

## 2.2. Heating and Cooling

The unloaded specimens were heated in an electric furnace according to the maximum temperature ( $T$ ). The typical temperature ( $T$ ) versus time ( $t$ ) relations recorded in the furnace were consistent with ISO834 standard heating curve [14]. The ambient temperature was about 20°C at the start of heating, the maximum temperature lasted for different hours for different specimens. At the end of heating, the furnace was switched off and the specimens were cooled down in the furnace with the door opened. The specimens after the elevated temperature exposure are shown in Fig. 1.

Specimens present different characteristics after exposed to high temperature as shown in Fig. 1. The color of the steel columns changed with the variation of the maximum temperatures. The color of specimens with the temperature of 400°C was yellowish-brown, the color of specimens with the temperatures of 550°C and 700°C was brick red, the color of specimens with the temperature of 1000°C was carbon black. High temperature duration has no evident influence on specimens with the temperatures of 400, 550, 700 and 1000°C. However, the color of the specimens with the temperature of 850°C changed with the increase of high temperature duration.

## 2.3. Compressive Tests

The compressive tests were carried out on a 1000 kN capacity testing machine. Figure 2 gives a schematic view of the test setup. Three locations with the interval of 90° at mid-height section of the specimens were selected to position the longitudinal and transverse strain gauges on the specimens, and a total of six strain gauges were used for each specimen, as shown in Fig. 3.  $\epsilon_1$  and  $\epsilon_2$  represent strains of the left flange strain measurement point,  $\epsilon_3$  and  $\epsilon_4$  represent strains of the web strain measurement point,  $\epsilon_5$  and  $\epsilon_6$  represent strains of the right flange strain measurement point.  $\epsilon_1$ ,  $\epsilon_3$  and  $\epsilon_5$  measure the longitudinal strain,  $\epsilon_2$ ,  $\epsilon_4$  and  $\epsilon_6$



**Figure 1. Specimens after heating and cooling.**

measure the transverse strain. During the tests, the strain was determined using a DH3816 Strain Measurement System.

The specimens were loaded with a speed of 1 kN/s continuously until the failure of specimens. A load interval of less than one tenth of the estimated ultimate strength was used, and each load interval was maintained for about 3 min to 4 min. The axial load versus displacement curve was obtained from the testing machine and the ultimate strength was recorded automatically.

#### **2.4. Failure Patterns**

It was found that the specimen's elevated temperatures had no influence on the failure patterns of the columns after compression test. The failure patterns of all the specimens were mainly due to local buckling. The two flange plates twisted towards while the axial load approach the ultimate load, at the same time, the upper part and the lower part of the web bulged to opposite directions. The deformation of flanges and web increased as the load increased until the failure of specimens. During the compression test, rust on the specimens with the temperature of 20, 400, 550 and 700°C and it's the same as the oxide layer on the specimens with the temperature of 850°C and 1000°C peeled off when the axial load achieved the yield load. The failure patterns of specimens are shown in Fig. 4.

#### **2.5. Load–Strain Response**

Figure 5 shows a group of load–strain curves of the specimens. Each of the figures is further divided into two parts to separately present the plots of transverse strain versus axial load to the left, and the plots of axial strain versus axial load to the right. The curves are consisted of three distinct stages, namely the first linear stage, the yielding process, and the hardening stage. In the first linear stage, the axial load is almost proportional to the strain (both axial strain and transverse strain) and the slope of the line is larger than that of the other two stages. This indicates that in the first linear stage, the deformations of the steel columns increased slowly with the increase of axial load and the deformation. The trans-

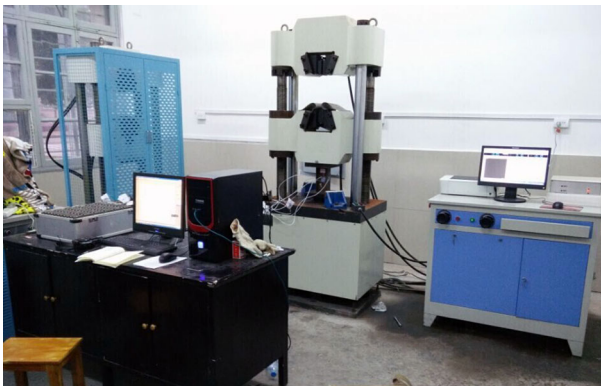


**Figure 2. Loading system.**

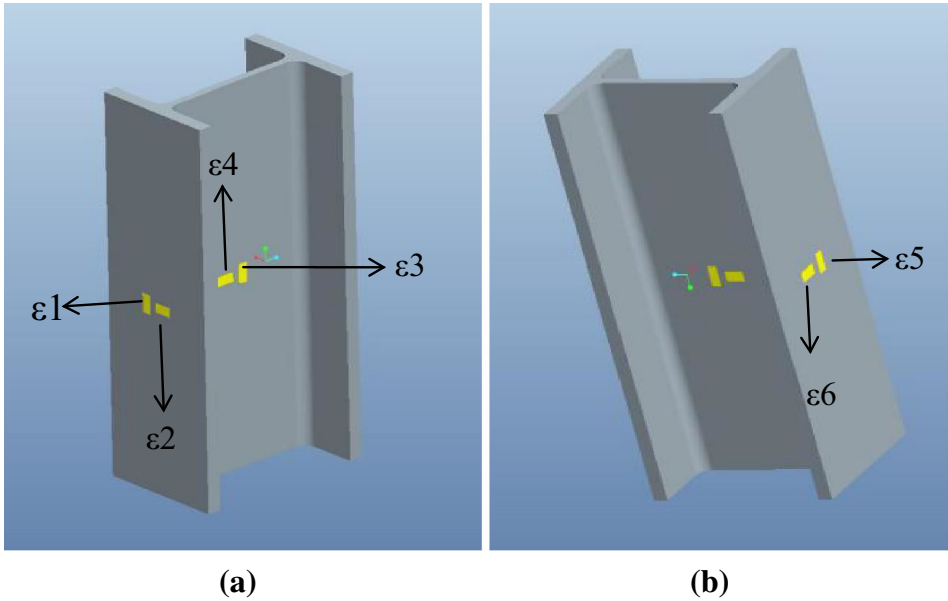


**Figure 3. Schematic view of the strain gauge location. (a) The left view, (b) the right view.**



**Figure 4. Typical failure modes of the specimens.**

verse strain is smaller than the axial strain with the same axial load in the first linear stage, this indicates that the transverse deformation is smaller than the axial deformation. In the yielding process, the steel column reached the yielding strain and the deformation began to increase fast though the axial load was not

increased. For each specimen, the axial load corresponding to the initial of yielding point of the three strain measurements is almost the same, this indicates that these strains entered the yielding process at the same time. After the yielding process, the hardening stage developed, which showed a positive stiffness with the deformation of axial strain rather than a softening behavior. In this stage, the deformation increased quickly with the increase of axial load.

High temperature duration has no effect on axial strain and lateral strain. The higher the temperature is, the earlier the strain points of specimen enter yield.

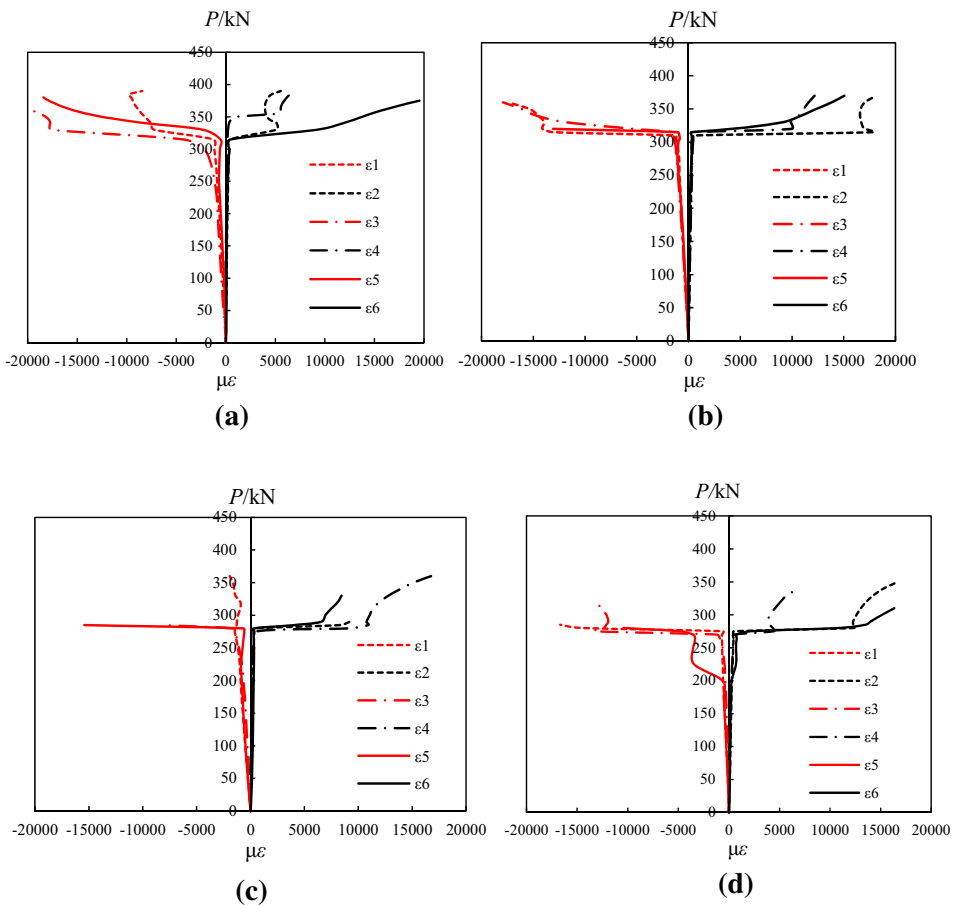


**Figure 5. Axial load ( $P$ ) versus strain ( $\epsilon$ ) relations of the specimens. (a)  $P$ - $\epsilon$  curve of specimen IT20t0, (b)  $P$ - $\epsilon$  curve of specimen IT550t0.5, (c)  $P$ - $\epsilon$  curve of specimen IT850t0.5, (d)  $P$ - $\epsilon$  curve of specimen IT850t2.5.**

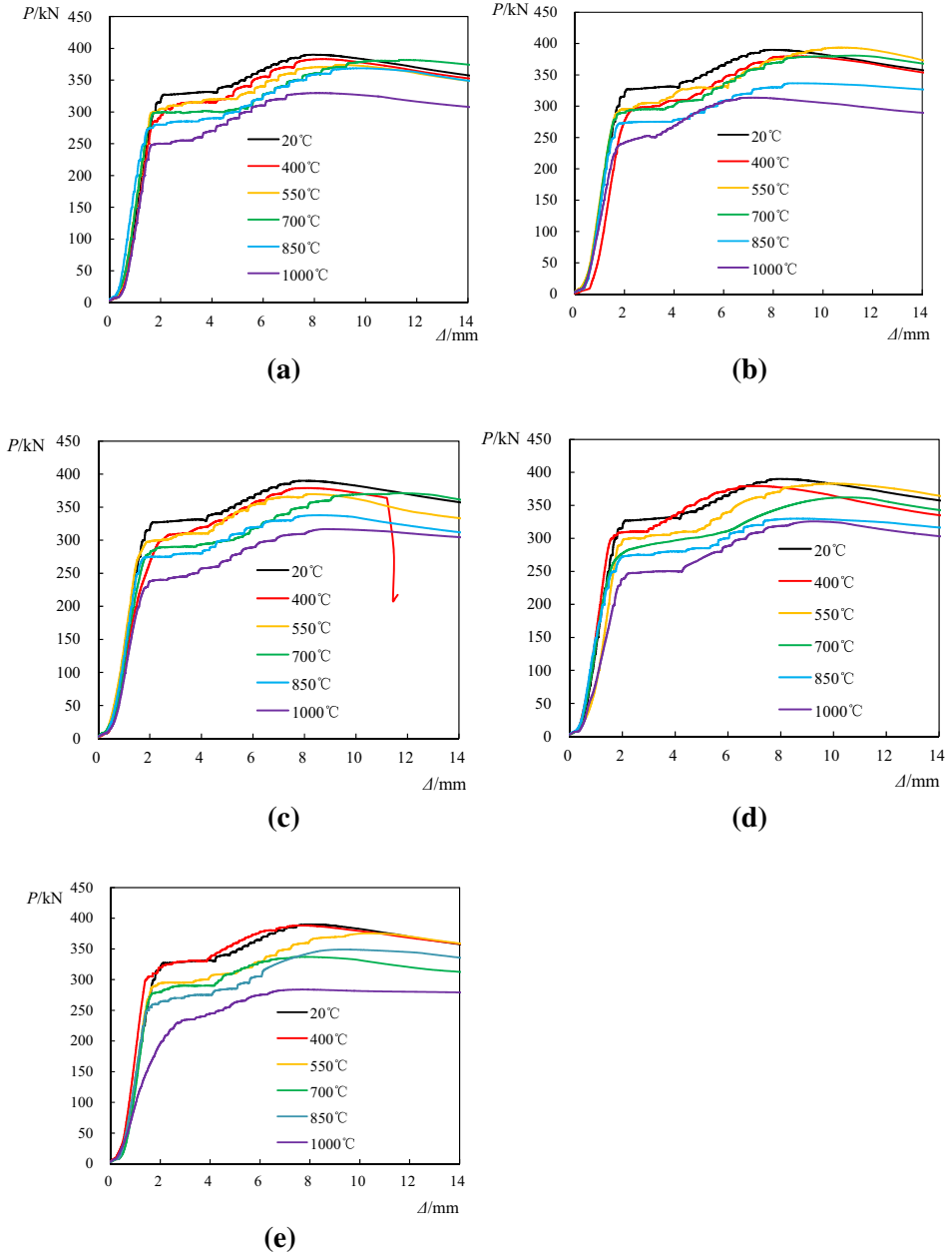


**Figure 6.  $P-\Delta$  curves of the specimens with different high temperature. (a)  $P-\Delta$  curve of specimens with  $t = 0.5$  h, (b)  $P-\Delta$  curve of specimens with  $t = 1.0$  h, (c)  $P-\Delta$  curve of specimens with  $t = 1.5$  h, (d)  $P-\Delta$  curve of specimens with  $t = 2.0$  h, (e)  $P-\Delta$  curve of specimens with  $t = 2.5$  h.**

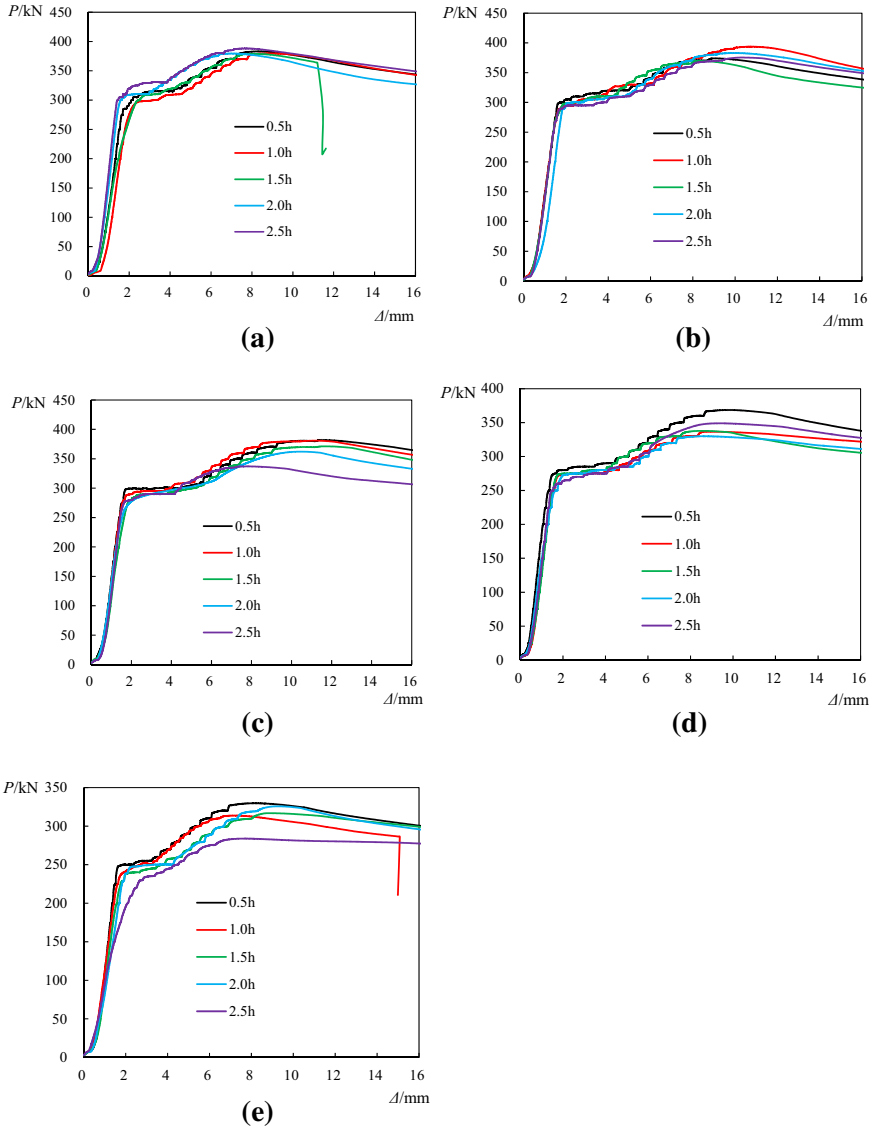


**Figure 7.  $P-\Delta$  curves of the specimens with different high temperature duration. (a)  $P-\Delta$  curve of specimens with  $T = 400^{\circ}\text{C}$ , (b)  $P-\Delta$  curve of specimens with  $T = 550^{\circ}\text{C}$ , (c)  $P-\Delta$  curve of specimens with  $T = 700^{\circ}\text{C}$ , (d)  $P-\Delta$  curve of specimens with  $T = 850^{\circ}\text{C}$ , (e)  $P-\Delta$  curve of specimens with  $T = 1000^{\circ}\text{C}$ .**

## 2.6. Load–Displacement Relationships

The axial load ( $P$ ) versus displacement ( $\Delta$ ) curves of specimens with different high temperatures are shown in Fig. 6. The axial load ( $P$ ) versus displacement ( $\Delta$ ) curves of specimens with different high temperature duration are shown in Fig. 7.

At the initial loading stage, the axial load versus displacement relation was generally linear. The initial stiffness ( $k$ ) of the specimens were determined as the unified secant slope where the axial load equals to the 50% yield load from the load–displacement curve. The yield load ( $P_y$ ) of the test specimens is defined as the axial load corresponding to the first turning point of the curve.

$\Delta_u$  is defined as the displacement of the test specimens corresponding to the ultimate load and  $\Delta_y$  is defined as the displacement of the test specimens corresponding to the yield load. The ductility coefficient of specimens is  $\Delta_u/\Delta_y$ .

Table 2 shows the initial stiffness, ductility coefficient, yield load and ultimate load of each specimen. It can be seen that, the high temperature exposure duration has limited effects on the initial stiffness, ductility coefficient, yield load and yield load to ultimate load ratio of each specimen. There is no evident reduction of the initial stiffness observed with the increase of the maximum temperature when the maximum temperatures were lower than 1000°C. The initial stiffness

**Table 2**  
**Test Results**

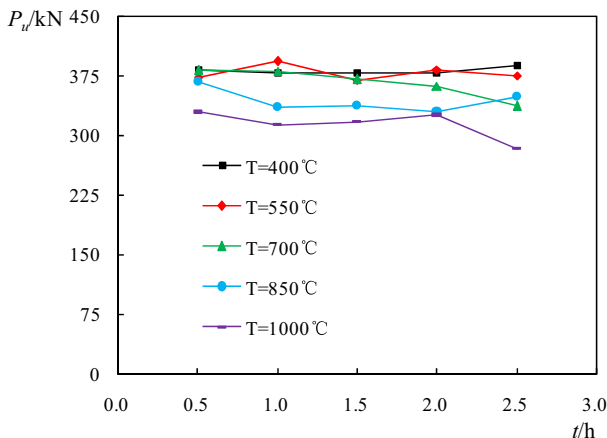
| Specimens  | $k$ (kN/mm) | $\Delta_u/\Delta_y$ | $P_y$ (kN) | $P_u$ (kN) | $P_y/P_u$ |
|------------|-------------|---------------------|------------|------------|-----------|
| IT20t0     | 252         | 3.95                | 323        | 389.95     | 0.83      |
| IT400t0.5  | 248         | 3.36                | 309        | 383.15     | 0.81      |
| IT400t1.0  | 230         | 3.71                | 301        | 379.65     | 0.79      |
| IT400t1.5  | 251         | 3.00                | 307        | 378.90     | 0.81      |
| IT400t2.0  | 242         | 3.89                | 306        | 379.40     | 0.81      |
| IT400t2.5  | 251         | 5.50                | 300        | 388.15     | 0.77      |
| IT550t0.5  | 257         | 5.56                | 303        | 373.95     | 0.81      |
| IT550t1.0  | 249         | 5.94                | 293        | 393.60     | 0.74      |
| IT550t1.5  | 232         | 4.42                | 298        | 369.70     | 0.81      |
| IT550t2.0  | 261         | 4.95                | 299        | 383.00     | 0.78      |
| IT550t2.5  | 226         | 5.37                | 293        | 375.35     | 0.78      |
| IT700t0.5  | 256         | 6.71                | 300        | 381.85     | 0.79      |
| IT700t1.0  | 226         | 5.29                | 293        | 380.70     | 0.77      |
| IT700t1.5  | 244         | 6.39                | 277        | 371.05     | 0.75      |
| IT700t2.0  | 243         | 6.50                | 263        | 362.05     | 0.73      |
| IT700t2.5  | 256         | 4.59                | 277        | 337.00     | 0.82      |
| IT850t0.5  | 206         | 6.47                | 274        | 368.60     | 0.74      |
| IT850t1.0  | 244         | 4.83                | 272        | 336.60     | 0.81      |
| IT850t1.5  | 248         | 4.72                | 273        | 337.80     | 0.81      |
| IT850t2.0  | 226         | 5.31                | 247        | 329.85     | 0.75      |
| IT850t2.5  | 202         | 5.81                | 255        | 348.95     | 0.73      |
| IT1000t0.5 | 198         | 5.06                | 247        | 329.70     | 0.75      |
| IT1000t1.0 | 193         | 3.79                | 240        | 313.65     | 0.76      |
| IT1000t1.5 | 206         | 4.40                | 237        | 316.75     | 0.75      |
| IT1000t2.0 | 201         | 4.79                | 227        | 325.65     | 0.70      |
| IT1000t2.5 | 190         | 2.66                | 233        | 283.85     | 0.82      |

reduced with a percentage of about 10% compared with that of specimens at ambient temperature when the maximum temperature reached 1000°C. It can also be found from Table 2 that the ductility coefficient was about 4 and the yield load to ultimate load ratio was about 0.8, no matter how high the maximum temperature was.

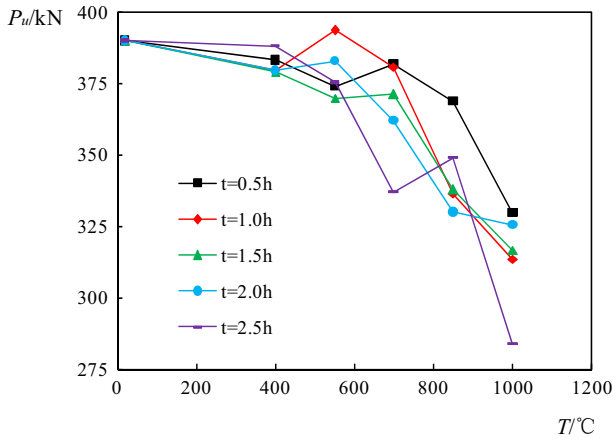
### 2.7. Analysis of the Ultimate Strength

Table 2 gives the measured ultimate strength ( $P_u$ ) of all specimens. Variations of the ultimate strength with high temperature duration ( $t$ ) curves of specimens exposure to different temperature exposure is shown in Fig. 8. It can be seen that the ultimate strength of specimens only fluctuate within a narrow range with variations of high temperature duration. This means that the high temperature duration has limited effects on the ultimate strength of the I-section steel columns. Figure 9 shows variations of the ultimate strength with different high temperature curves of specimens under different high temperature duration. It can be seen that, the ultimate strength decreases with the increase of the high temperature exposure, the higher the specimen temperature, the faster the ultimate strength decline.

The average ultimate strength of specimens with different high temperature durations while with the same high temperature is representative of a certain temperature because the ultimate strength of specimens after reaching a high temperature is approximately constant no matter how the high temperature duration varies.  $P_0$  is defined as the ultimate strength of specimen IT20t0 and  $P_1$  is defined as the average ultimate strength of specimens at a certain temperature.  $\gamma$  is defined as the remaining load bearing capacity coefficient and can be expressed as  $\gamma = P_1/P_0$ . Table 3 shows the average strength and the remaining bearing capacity coefficient. Average strength and the remaining bearing capacity coefficient of I-section steel short columns after elevated temperature decrease with the increase of high temperature.



**Figure 8.**  $P_u$ - $t$  relations of the specimens.



**Figure 9.**  $P_u$ - $T$  relations of the specimens.

**Table 3**  
**Summary of Average Ultimate Strength**

| Temperature (°C)               | 20     | 400    | 550    | 700    | 850    | 1000   |
|--------------------------------|--------|--------|--------|--------|--------|--------|
| Average ultimate strength (kN) | 389.95 | 381.85 | 379.12 | 366.53 | 343.34 | 313.92 |
| $\gamma$                       | 1.00   | 0.98   | 0.97   | 0.94   | 0.88   | 0.81   |

### 3. Calibration Study

#### 3.1. Material Properties

Different specimen elevated temperatures may induce variations in the post-high temperature mechanical properties [15]. In order to evaluate the mechanical properties of steel after reaching an elevated temperature, eighteen basic tensile coupon tests (every three for a certain temperature) were conducted in accordance with GB/T 228-2002 [16]. Coupons were taken from the flange and web of I-section Q235 steel section. Before the tensile coupon tests, coupons were heated to a target high temperature and cooled down to the ambient temperature. Associated

**Table 4**  
**Material Properties of Q235 Steel After Different High Temperatures**

| $T$ (°C) | $f_y$ (Mpa) | $f_u$ (Mpa) | $\delta$ (%) | $E$ (Gpa) |
|----------|-------------|-------------|--------------|-----------|
| 20       | 235         | 390         | 30           | 210       |
| 400      | 225         | 386         | 29           | 205       |
| 550      | 220         | 377         | 31           | 207       |
| 700      | 211         | 365         | 33           | 209       |
| 850      | 197         | 357         | 27           | 204       |

mechanical properties are obtained, including yield strengths ( $f_y$ ), ultimate strengths ( $f_u$ ), elongation ( $\delta$ ) and elastic modulus ( $E$ ), as shown in Table 4.

### 3.2. FEA Model

The Finite Element Analysis (FEA) software ABAQUS was used for a numerical investigation mechanical behaviour of I-section steel short columns after elevated temperature under compression [17]. The steel material properties and cross-section dimensions obtained from the experiments were used input to the FEA. In order to model the I-section steel short columns, three-dimensional eight-node solid element C3D8I was used in this numerical study. The finite element meshes of joints are shown in Fig. 10b for the I-section steel short columns. A convergence study was done by comparing FEA results with test results. A convergence study was conducted to obtain a suitable mesh size for modeling the I-section steel short columns specimens before the FE model was used to carry out the following analyses.

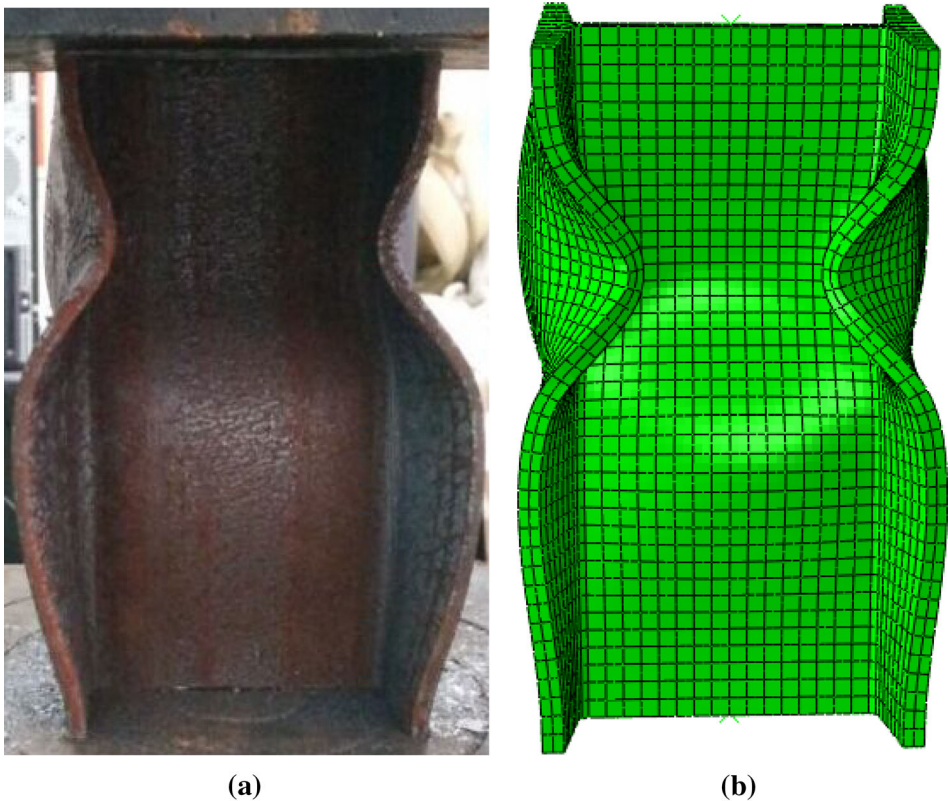


**Figure 10. Comparison of the failure patterns between test and FEA. (a) Failure pattern in test, (b) failure pattern in FEA.**

The web and flange of I-section steel short columns were divided into two layers in the thickness direction in the FEA models, as shown in Fig. 10b. It was found that the two-element mesh density in the thickness direction of web and flange could achieve accurate results with minimum computational time by using FEA validation. Finite element analysis of the twenty six specimens was carried out in accordance with the above mesh density of finite element simulation. Loading and boundary conditions were the same as the test. Both ends of the I-section steel short columns were pinned to simulate the boundary conditions in the test by releasing the rotational constraint. The compressive force in I-section steel short columns was simulated as surface pressure in the FEA model.

The width and length of control element of web and flanges of I-section steel short columns were arranged at about 3 mm. The total number of elements in I-section steel short columns FE model was about 5000. The number of elements in the two flanges was about 45% of total number of element.

### 3.3. Validation

The comparison of the column failure pattern predicted in the finite element analysis with the failure pattern of the columns observed in the test is shown in Fig. 10. It can be seen that the failure pattern predicted from the model matches well with those observed in test.

The ultimate strength predicted from the finite element analysis is also compared with that measured in tests, as shown in Table 5. It can be seen that the load bearing capacity predicted from analysis is generally in good agreement with that measured in tests with a maximum difference of 11% and average difference of 3%. These good agreements indicate that the FEA model is capable of predicting the ultimate strength of I-section steel short columns after high temperature and can be used for undertaking a detailed parameter investigation on the factors governing the ultimate strength of I-section steel short columns.

## 4. Parametric Study

### 4.1. Influential Parameters

Parametric investigations were carried out to study the effects of three parameters (high temperature  $T$ , height-to-thickness ratio of web  $\alpha$  and width-to-thickness ratio of flange  $\beta$ ) on the mechanical behaviors of the I-section steel columns after elevated temperature. Values of the three parameters are shown in Table 6. 64 I-section steel short columns after elevated temperature with different parameters were analyzed to obtain the ultimate strength, as shown in Table 7. The identical element type, mesh size and material modeling of I-section steel short columns used in the validation study were also employed in the parametric study. The two ends of columns were modeled by using the pinned connection in the parametric study.

The invariant dimensions are: height of web  $h = 220$  mm, width of flange  $b = 110$  mm and height of specimens  $L = 500$  mm. All the cross sections of the

**Table 5**  
**Comparison of the Ultimate Strength**

| Label      | Ultimate strength (kN) |                        | Deviation (%) |
|------------|------------------------|------------------------|---------------|
|            | Observed in tests      | Predicted by the model |               |
| IT20t0     | 390.0                  | 391.7                  | 0.4           |
| IT400t0.5  | 383.2                  | 385.8                  | 0.7           |
| IT400t1.0  | 379.7                  | 385.8                  | 1.6           |
| IT400t1.5  | 378.9                  | 385.8                  | 1.8           |
| IT400t2.0  | 379.4                  | 385.8                  | 1.7           |
| IT400t2.5  | 388.2                  | 385.8                  | 0.6           |
| IT550t0.5  | 374.0                  | 376.9                  | 0.8           |
| IT550t1.0  | 393.6                  | 376.9                  | 4.2           |
| IT550t1.5  | 369.7                  | 376.9                  | 1.9           |
| IT550t2.0  | 383.0                  | 376.9                  | 1.6           |
| IT550t2.5  | 375.4                  | 376.9                  | 0.4           |
| IT700t0.5  | 381.9                  | 366.7                  | 4.0           |
| IT700t1.0  | 380.7                  | 366.7                  | 3.7           |
| IT700t1.5  | 371.1                  | 366.7                  | 1.2           |
| IT700t2.0  | 362.1                  | 366.7                  | 1.3           |
| IT700t2.5  | 337.0                  | 366.7                  | 8.8           |
| IT850t0.5  | 368.6                  | 348.8                  | 5.4           |
| IT850t1.0  | 336.6                  | 348.8                  | 3.6           |
| IT850t1.5  | 337.8                  | 348.8                  | 3.3           |
| IT850t2.0  | 329.9                  | 348.8                  | 5.7           |
| IT850t2.5  | 349.0                  | 348.8                  | 0.1           |
| IT1000t0.5 | 329.7                  | 314.6                  | 4.6           |
| IT1000t1.0 | 313.7                  | 314.6                  | 0.3           |
| IT1000t1.5 | 316.8                  | 314.6                  | 0.7           |
| IT1000t2.0 | 325.7                  | 314.6                  | 3.4           |
| IT1000t2.5 | 283.9                  | 314.6                  | 10.8          |

**Table 6**  
**Details of Parameters in FEA**

| Parameters $T$ (°C) | Values of parameters |     |     |     |
|---------------------|----------------------|-----|-----|-----|
|                     | 20                   | 550 | 700 | 850 |
| $\alpha$            | 16                   | 24  | 32  | 40  |
| $\beta$             | 5                    | 9   | 13  | 17  |

columns in FEA were classified as class 1 according to Eurocode 3. The labels of element models are consist of four parts, for example, label  $\alpha 16\beta 5T550$  contains the following information: type of cross section is I-section, height-to-thickness ratio of web is  $\alpha = 16$ , width-to-thickness ratio of flange is  $\beta = 5$  and high temperature specimens suffered is  $T = 550^\circ\text{C}$ . Details of the models are listed in Table 7.

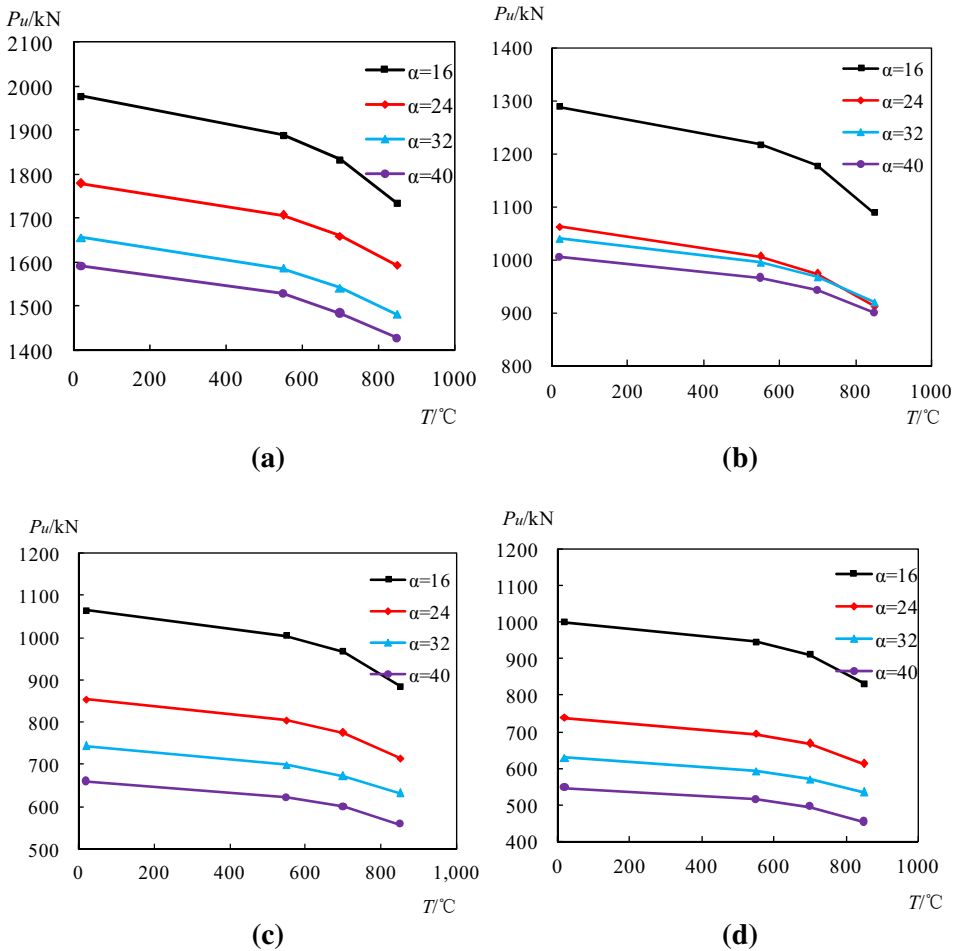


**Figure 11. Ultimate strength versus high temperature curves. (a)  $P_u$ - $T$  curve with  $\beta = 5$ , (b)  $P_u$ - $T$  curve with  $\beta = 9$ , (c)  $P_u$ - $T$  curve with  $\beta = 13$ , (d)  $P_u$ - $T$  curve with  $\beta = 17$ .**

#### 4.2. Effect of High Temperature

Figure 11 shows variations of the ultimate strength with different high temperature curves of finite element models of columns under different height-to-thickness ratio of web and different width-to-thickness ratio of flange.

It can be seen that the specimens' ultimate strengths decrease remarkably with the increase of the high temperature specimens suffered. What's more, the higher the temperature is, the faster the ultimate strength of columns declines. The relations between ultimate strength and high temperature are consistent under different height-to-thickness ratio of web and different width-to-thickness ratio of

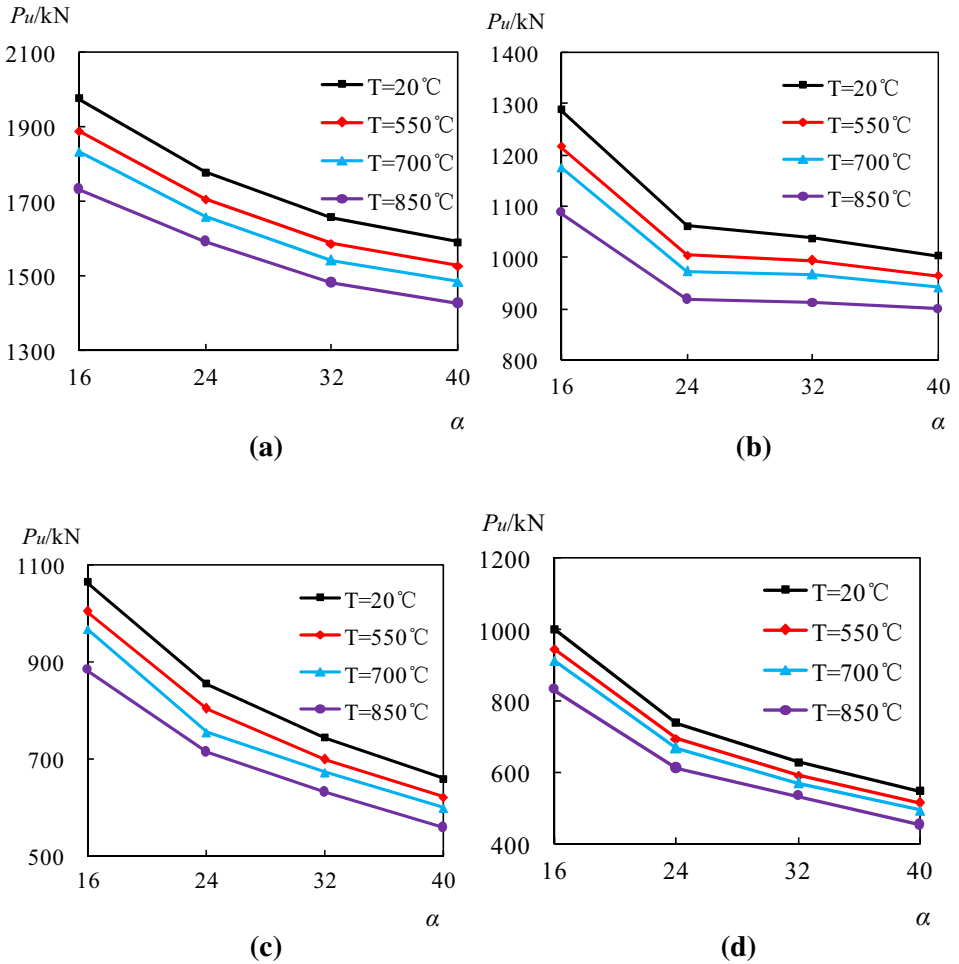


**Figure 12. Ultimate strength versus height-to-thickness ratio curves. (a)  $P_u$ - $\alpha$  curve with  $\beta = 5$ , (b)  $P_u$ - $\alpha$  curve with  $\beta = 9$ , (c)  $P_u$ - $\alpha$  curve with  $\beta = 13$ , (d)  $P_u$ - $\alpha$  curve with  $\beta = 17$ .**

flange. When the high temperatures are 550, 700 and  $850^\circ\text{C}$ , the ultimate strength decrease by 4, 7, and 12% compared to that at ambient temperature, respectively.

### 4.3. Effect of Height-to-Thickness Ratio

Figure 12 shows variations of the ultimate strength of columns with different height-to-thickness ratio of web curves of finite element models.

It can be found that the relations between ultimate strength and height-to-thickness ratio of web are consistent under different elevated temperatures but the same width-to-thickness ratio of the flange. From Fig. 12a, when the height-to-thickness ratio of the web is 24, the ultimate strength decreases by 10% compared

**Table 7**  
**Details of Finite Element Models**

| Models                       | $\alpha$ | $\beta$ | $T$ (°C) | $F_m$ (kN) | $F_u$ (kN) | $F_m/F_u$ |
|------------------------------|----------|---------|----------|------------|------------|-----------|
| I $\alpha$ 16 $\beta$ 5T20   | 16       | 5       | 20       | 1977.8     | 1898.4     | 1.04      |
| I $\alpha$ 16 $\beta$ 5T550  | 16       | 5       | 550      | 1889.6     | 1765.8     | 1.07      |
| I $\alpha$ 16 $\beta$ 5T700  | 16       | 5       | 700      | 1833.9     | 1683.6     | 1.09      |
| I $\alpha$ 16 $\beta$ 5T850  | 16       | 5       | 850      | 1733.3     | 1581.5     | 1.10      |
| I $\alpha$ 16 $\beta$ 9T20   | 16       | 9       | 20       | 1289.0     | 1379.2     | 0.93      |
| I $\alpha$ 16 $\beta$ 9T550  | 16       | 9       | 550      | 1217.9     | 1282.9     | 0.95      |
| I $\alpha$ 16 $\beta$ 9T700  | 16       | 9       | 700      | 1177.1     | 1223.1     | 0.96      |
| I $\alpha$ 16 $\beta$ 9T850  | 16       | 9       | 850      | 1088.5     | 1149.0     | 0.95      |
| I $\alpha$ 16 $\beta$ 13T20  | 16       | 13      | 20       | 1065.9     | 1179.5     | 0.90      |
| I $\alpha$ 16 $\beta$ 13T550 | 16       | 13      | 550      | 1004.6     | 1097.1     | 0.92      |
| I $\alpha$ 16 $\beta$ 13T700 | 16       | 13      | 700      | 968.7      | 1046.0     | 0.93      |
| I $\alpha$ 16 $\beta$ 13T850 | 16       | 13      | 850      | 885.1      | 982.6      | 0.90      |
| I $\alpha$ 16 $\beta$ 17T20  | 16       | 17      | 20       | 1001.9     | 1073.8     | 0.93      |
| I $\alpha$ 16 $\beta$ 17T550 | 16       | 17      | 550      | 946.9      | 998.8      | 0.95      |
| I $\alpha$ 16 $\beta$ 17T700 | 16       | 17      | 700      | 913.4      | 952.2      | 0.96      |
| I $\alpha$ 16 $\beta$ 17T850 | 16       | 17      | 850      | 833.9      | 894.5      | 0.93      |
| I $\alpha$ 24 $\beta$ 5T20   | 24       | 5       | 20       | 1779.7     | 1655.0     | 1.08      |
| I $\alpha$ 24 $\beta$ 5T550  | 24       | 5       | 550      | 1707.1     | 1539.5     | 1.11      |
| I $\alpha$ 24 $\beta$ 5T700  | 24       | 5       | 700      | 1660.5     | 1467.7     | 1.13      |
| I $\alpha$ 24 $\beta$ 5T850  | 24       | 5       | 850      | 1593.3     | 1378.8     | 1.16      |
| I $\alpha$ 24 $\beta$ 9T20   | 24       | 9       | 20       | 1062.1     | 1135.8     | 0.94      |
| I $\alpha$ 24 $\beta$ 9T550  | 24       | 9       | 550      | 1005.8     | 1056.5     | 0.95      |
| I $\alpha$ 24 $\beta$ 9T700  | 24       | 9       | 700      | 973.3      | 1007.3     | 0.97      |
| I $\alpha$ 24 $\beta$ 9T850  | 24       | 9       | 850      | 919.2      | 946.2      | 0.97      |
| I $\alpha$ 24 $\beta$ 13T20  | 24       | 13      | 20       | 855.0      | 936.1      | 0.91      |
| I $\alpha$ 24 $\beta$ 13T550 | 24       | 13      | 550      | 804.7      | 870.7      | 0.92      |
| I $\alpha$ 24 $\beta$ 13T700 | 24       | 13      | 700      | 775.0      | 830.2      | 0.93      |
| I $\alpha$ 24 $\beta$ 13T850 | 24       | 13      | 850      | 715.3      | 779.8      | 0.92      |
| I $\alpha$ 24 $\beta$ 17T20  | 24       | 17      | 20       | 740.1      | 830.4      | 0.89      |
| I $\alpha$ 24 $\beta$ 17T550 | 24       | 17      | 550      | 695.8      | 772.4      | 0.90      |
| I $\alpha$ 24 $\beta$ 17T700 | 24       | 17      | 700      | 669.2      | 736.4      | 0.91      |
| I $\alpha$ 24 $\beta$ 17T850 | 24       | 17      | 850      | 613.4      | 691.8      | 0.89      |
| I $\alpha$ 32 $\beta$ 5T20   | 32       | 5       | 20       | 1656.6     | 1533.3     | 1.08      |
| I $\alpha$ 32 $\beta$ 5T550  | 32       | 5       | 550      | 1587.1     | 1426.3     | 1.11      |
| I $\alpha$ 32 $\beta$ 5T700  | 32       | 5       | 700      | 1542.1     | 1359.8     | 1.13      |
| I $\alpha$ 32 $\beta$ 5T850  | 32       | 5       | 850      | 1481.9     | 1277.4     | 1.16      |
| I $\alpha$ 32 $\beta$ 9T20   | 32       | 9       | 20       | 1039.2     | 1014.1     | 1.02      |
| I $\alpha$ 32 $\beta$ 9T550  | 32       | 9       | 550      | 995.1      | 943.3      | 1.05      |
| I $\alpha$ 32 $\beta$ 9T700  | 32       | 9       | 700      | 967.5      | 899.3      | 1.08      |
| I $\alpha$ 32 $\beta$ 9T850  | 32       | 9       | 850      | 911.8      | 844.8      | 1.08      |
| I $\alpha$ 32 $\beta$ 13T20  | 32       | 13      | 20       | 744.1      | 814.4      | 0.91      |
| I $\alpha$ 32 $\beta$ 13T550 | 32       | 13      | 550      | 699.9      | 757.5      | 0.92      |
| I $\alpha$ 32 $\beta$ 13T700 | 32       | 13      | 700      | 673.5      | 722.2      | 0.93      |
| I $\alpha$ 32 $\beta$ 13T850 | 32       | 13      | 850      | 632.7      | 678.5      | 0.93      |
| I $\alpha$ 32 $\beta$ 17T20  | 32       | 17      | 20       | 630.8      | 708.7      | 0.89      |
| I $\alpha$ 32 $\beta$ 17T550 | 32       | 17      | 550      | 593.9      | 659.2      | 0.90      |
| I $\alpha$ 32 $\beta$ 17T700 | 32       | 17      | 700      | 571.1      | 628.5      | 0.91      |
| I $\alpha$ 32 $\beta$ 17T850 | 32       | 17      | 850      | 535.6      | 590.4      | 0.91      |

**Table 7**  
**continued**

| Models                       | $\alpha$ | $\beta$ | $T$ (°C) | $F_m$ (kN) | $F_u$ (kN) | $F_m/F_u$ |
|------------------------------|----------|---------|----------|------------|------------|-----------|
| I $\alpha$ 40 $\beta$ 5T20   | 40       | 5       | 20       | 1591.5     | 1460.3     | 1.09      |
| I $\alpha$ 40 $\beta$ 5T550  | 40       | 5       | 550      | 1528.3     | 1358.3     | 1.13      |
| I $\alpha$ 40 $\beta$ 5T700  | 40       | 5       | 700      | 1485.0     | 1295.0     | 1.15      |
| I $\alpha$ 40 $\beta$ 5T850  | 40       | 5       | 850      | 1426.9     | 1216.6     | 1.17      |
| I $\alpha$ 40 $\beta$ 9T20   | 40       | 9       | 20       | 1004.3     | 941.1      | 1.07      |
| I $\alpha$ 40 $\beta$ 9T550  | 40       | 9       | 550      | 965.7      | 875.4      | 1.10      |
| I $\alpha$ 40 $\beta$ 9T700  | 40       | 9       | 700      | 941.8      | 834.6      | 1.13      |
| I $\alpha$ 40 $\beta$ 9T850  | 40       | 9       | 850      | 900.1      | 784.0      | 1.15      |
| I $\alpha$ 40 $\beta$ 13T20  | 40       | 13      | 20       | 661.0      | 741.4      | 0.89      |
| I $\alpha$ 40 $\beta$ 13T550 | 40       | 13      | 550      | 622.9      | 689.6      | 0.90      |
| I $\alpha$ 40 $\beta$ 13T700 | 40       | 13      | 700      | 600.5      | 657.5      | 0.91      |
| I $\alpha$ 40 $\beta$ 13T850 | 40       | 13      | 850      | 559.4      | 617.6      | 0.91      |
| I $\alpha$ 40 $\beta$ 17T20  | 40       | 17      | 20       | 547.7      | 635.7      | 0.86      |
| I $\alpha$ 40 $\beta$ 17T550 | 40       | 17      | 550      | 515.6      | 591.3      | 0.87      |
| I $\alpha$ 40 $\beta$ 17T700 | 40       | 17      | 700      | 496.0      | 563.7      | 0.88      |
| I $\alpha$ 40 $\beta$ 17T850 | 40       | 17      | 850      | 455.0      | 529.6      | 0.86      |

to a ratio of 16; when the height-to-thickness ratio of the web is 32, the ultimate strength decreases by 7% compared to that a ratio of 24; when the height-to-thickness ratio of the web is 40, the ultimate strength decreased by 3% compared to a ratio of 32. From Fig. 12b, it can be found that when height-to-thickness ratio of the web is 24, the ultimate strength decreases by 18% compared to a ratio of 16; when the height-to-thickness ratio of the web is 32, the ultimate strength decreases by 2% compared to a ratio of 24; when the height-to-thickness ratio of the web is 40, the ultimate strength decreases by 3% compared to a ratio of 32. From Fig. 12c, it can be found that when the height-to-thickness ratio of the web is 24, the ultimate strength decreases by 19% compared to a ratio of 16; when height-to-thickness ratio of the web is 32, the ultimate strength decreases by 10% compared to a ratio of 24; when the height-to-thickness ratio of the web is 40, the ultimate strength decreases by 10% compared to a ratio of 32. From Fig. 12d, it can be found that when the height-to-thickness ratio of the web is 24, the ultimate strength decreases by 26% compared to a ratio of 16; when the height-to-thickness ratio of the web is 32, the ultimate strength decreases by 14% compared to a ratio of 24; when the height-to-thickness ratio of the web is 40, the ultimate strength decreases by 14% compared to a ratio of 32. It can be seen that with an increase of web height-to-thickness ratio, the ultimate strength decreases. The smaller web's height-to-thickness ratio of web is, the faster the ultimate strength of the columns increase.

#### 4.4. Effect of Width-to-Thickness Ratio

Figure 13 shows variations of the ultimate strength with different width-to-thickness ratio of flange curves of finite element models.

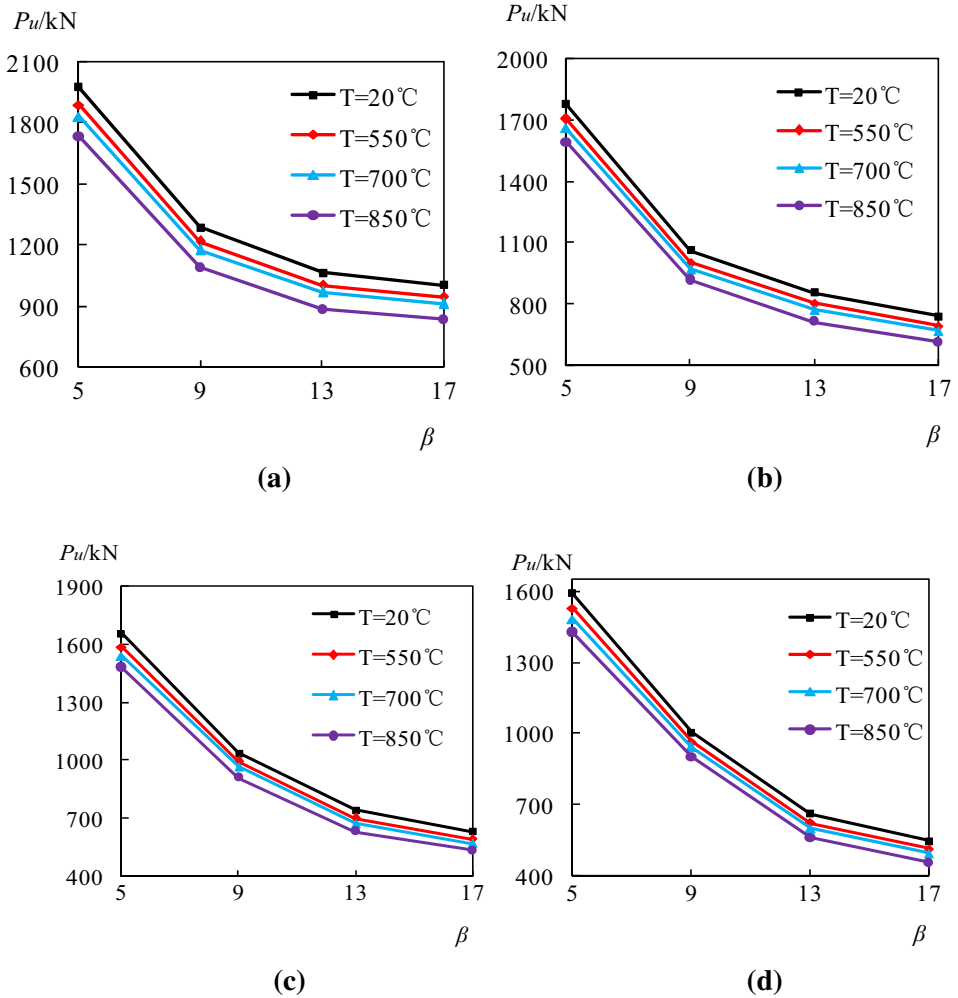


**Figure 13. Ultimate strength versus width-to-thickness ratio curves. (a)  $P_u$ - $\beta$  curve with  $\alpha = 16$ , (b)  $P_u$ - $\beta$  curve with  $\alpha = 24$ , (c)  $P_u$ - $\beta$  curve with  $\alpha = 32$ , (d)  $P_u$ - $\beta$  curve with  $\alpha = 40$ .**

The relationship between the ultimate strength and width-to-thickness ratio of the flange are consistent under different high temperatures but the same height-to-thickness ratio of web. From Fig. 13a, it can be found that when the width-to-thickness ratio of the flange is 9, the ultimate strength decreases by 35% compared to when the ratio is 5; when the width-to-thickness ratio of the flange is 13, the ultimate strength decreases by 17% compared to when the ratio is 9; when the width-to-thickness ratio of the flange is 17, the ultimate strength decreases by 6% compared to when the ratio is 13. From Fig. 13b, it can be found that when the width-to-thickness ratio of flange is 9, the ultimate strength decrease by 40% com-

pared to when the ratio is 5; when the width-to-thickness ratio of the flange is 13, the ultimate strength decreases by 20% compared to when the ratio is 9; when the width-to-thickness ratio of the flange is 17, the ultimate strength decreases by 13% compared to when the ratio is 13. From Fig. 13c, it can be found that when the width-to-thickness ratio of flange is 9, the ultimate strength decreases by 37% compared to when the ratio is 5; when the width-to-thickness ratio of flange is 13, the ultimate strength decreases by 28% compared to when the ratio is 9; when the width-to-thickness ratio of the flange is 17, the ultimate strength decrease by 15% compared to when the ratio is 13. From Fig. 13d, it can be found that when the width-to-thickness ratio of the flange is 9, the ultimate strength decreases by 36% compared to when the ratio is 5; when the width-to-thickness ratio of the flange is 13, the ultimate strength decrease by 34% compared to when the ratio is 9; when the width-to-thickness ratio of the flange is 17, the ultimate strength decrease by 17% compared to when the ratio is 13. It can be seen that with the increase of the width-to-thickness ratio of the flange, the ultimate strength decreases. The smaller width-to-thickness ratio of the flange is, the faster the ultimate strength of columns increase.

#### 4.5. Predictive Formula

At present, there is no formula available for the residual strength of I-section steel short columns after reaching a high temperature. Thus, a new predictive formula with considerable precision yet simple in form has been proposed to evaluate the ultimate strength of I-section steel short columns after reaching high temperatures based on the numerical simulation in this paper. As the maximum temperature  $T$ , height-to-thickness ratio of web  $\alpha$  and width-to-thickness ratio of flange  $\beta$  are the main factors for determining the ultimate strength, the predictive formula is developed as a function of  $T$ ,  $\alpha$  and  $\beta$ . The formula of strength for I-section steel short columns after high temperature under axial loading is given as follows:

$$F_u = \left[ -2.37 \times 10^{-10} \times \left( \frac{T}{T_0} \right)^2 + 4.81 \times 10^{-8} \times \left( \frac{T}{T_0} \right) + 1.03 \times 10^{-3} \right] \times f_{y0} \times \left( \frac{h^2}{\alpha} + 2 \times \frac{b^2}{\beta} \right) \quad (1)$$

**Table 8**  
**Comparison of the Calculated and Experimental Ultimate Strength of I-Section Steel Short Columns**

| 64 specimens | Comparison of $F_m$ and $F_u$ |
|--------------|-------------------------------|
| Max value    | 1.170                         |
| Min value    | 0.860                         |
| Mean value   | 0.987                         |
| COV          | 0.009                         |
| SD           | 0.095                         |

- $F_u$  is the calculated ultimate load.
- $T$  is the maximum temperature and  $T_0$  is “20°C”.  $T$  is measured in °C.
- $\alpha$  is height-to-thickness ratio of web and  $\beta$  is width-to-thickness ratio of flange.
- $h$  is height of web and  $b$  is width of flange.
- $f_{y0}$  is yield strength of steel under room temperature.

**Table 9**  
**Details of the Long Columns with Different Slenderness Ratio**

| Label             | Overall length (mm) | $\lambda$ | T   | Failure modes | $N_m$ | $\psi_m$ | $\psi_u$ | $\psi_m/\psi_u$ |
|-------------------|---------------------|-----------|-----|---------------|-------|----------|----------|-----------------|
| $\lambda 25T20$   | 625                 | 25        | 20  | Mode one      | 647.4 | 0.89     | 0.95     | 0.94            |
| $\lambda 50T20$   | 1250                | 50        | 20  | Mode two      | 593.4 | 0.82     | 0.86     | 0.96            |
| $\lambda 75T20$   | 1875                | 75        | 20  | Mode three    | 512.7 | 0.71     | 0.72     | 0.98            |
| $\lambda 100T20$  | 2500                | 100       | 20  | Mode three    | 404.6 | 0.56     | 0.55     | 1.01            |
| $\lambda 125T20$  | 3125                | 125       | 20  | Mode three    | 290.7 | 0.40     | 0.41     | 0.98            |
| $\lambda 150T20$  | 3750                | 150       | 20  | Mode three    | 224.2 | 0.31     | 0.31     | 1.01            |
| $\lambda 175T20$  | 4375                | 175       | 20  | Mode three    | 175.2 | 0.24     | 0.24     | 1.03            |
| $\lambda 200T20$  | 5000                | 200       | 20  | Mode three    | 137.9 | 0.19     | 0.19     | 1.02            |
| $\lambda 225T20$  | 5625                | 225       | 20  | Mode three    | 112.7 | 0.16     | 0.15     | 1.04            |
| $\lambda 250T20$  | 6250                | 250       | 20  | Mode three    | 92.8  | 0.13     | 0.12     | 1.04            |
| $\lambda 25T550$  | 625                 | 25        | 550 | Mode one      | 609.3 | 0.90     | 0.96     | 0.94            |
| $\lambda 50T550$  | 1250                | 50        | 550 | Mode two      | 572.0 | 0.84     | 0.86     | 0.98            |
| $\lambda 75T550$  | 1875                | 75        | 550 | Mode three    | 465.0 | 0.69     | 0.73     | 0.93            |
| $\lambda 100T550$ | 2500                | 100       | 550 | Mode three    | 386.4 | 0.57     | 0.58     | 0.99            |
| $\lambda 125T550$ | 3125                | 125       | 550 | Mode three    | 279.5 | 0.41     | 0.43     | 0.96            |
| $\lambda 150T550$ | 3750                | 150       | 550 | Mode three    | 218.1 | 0.32     | 0.32     | 0.99            |
| $\lambda 175T550$ | 4375                | 175       | 550 | Mode three    | 174.9 | 0.26     | 0.25     | 1.03            |
| $\lambda 200T550$ | 5000                | 200       | 550 | Mode three    | 136.7 | 0.20     | 0.20     | 1.02            |
| $\lambda 225T550$ | 5625                | 225       | 550 | Mode three    | 111.4 | 0.16     | 0.16     | 1.03            |
| $\lambda 250T550$ | 6250                | 250       | 550 | Mode three    | 92.0  | 0.14     | 0.13     | 1.04            |
| $\lambda 25T700$  | 625                 | 25        | 700 | Mode one      | 586.7 | 0.90     | 0.96     | 0.94            |
| $\lambda 50T700$  | 1250                | 50        | 700 | Mode two      | 513.2 | 0.79     | 0.87     | 0.91            |
| $\lambda 75T700$  | 1875                | 75        | 700 | Mode three    | 475.2 | 0.73     | 0.75     | 0.98            |
| $\lambda 100T700$ | 2500                | 100       | 700 | Mode three    | 348.9 | 0.54     | 0.59     | 0.91            |
| $\lambda 125T700$ | 3125                | 125       | 700 | Mode three    | 272.9 | 0.42     | 0.45     | 0.94            |
| $\lambda 150T700$ | 3750                | 150       | 700 | Mode three    | 214.0 | 0.33     | 0.34     | 0.98            |
| $\lambda 175T700$ | 4375                | 175       | 700 | Mode three    | 174.3 | 0.27     | 0.26     | 1.03            |
| $\lambda 200T700$ | 5000                | 200       | 700 | Mode three    | 136.6 | 0.21     | 0.21     | 1.02            |
| $\lambda 225T700$ | 5625                | 225       | 700 | Mode three    | 111.4 | 0.17     | 0.17     | 1.03            |
| $\lambda 250T700$ | 6250                | 250       | 700 | Mode three    | 91.5  | 0.14     | 0.14     | 1.03            |
| $\lambda 25T850$  | 625                 | 25        | 850 | Mode one      | 551.8 | 0.91     | 0.96     | 0.95            |
| $\lambda 50T850$  | 1250                | 50        | 850 | Mode two      | 496.5 | 0.82     | 0.87     | 0.94            |
| $\lambda 75T850$  | 1875                | 75        | 850 | Mode three    | 420.3 | 0.69     | 0.76     | 0.91            |
| $\lambda 100T850$ | 2500                | 100       | 850 | Mode three    | 347.1 | 0.57     | 0.61     | 0.94            |
| $\lambda 125T850$ | 3125                | 125       | 850 | Mode three    | 262.4 | 0.43     | 0.47     | 0.93            |
| $\lambda 150T850$ | 3750                | 150       | 850 | Mode three    | 206.8 | 0.34     | 0.35     | 0.96            |
| $\lambda 175T850$ | 4375                | 175       | 850 | Mode three    | 172.8 | 0.28     | 0.27     | 1.04            |
| $\lambda 200T850$ | 5000                | 200       | 850 | Mode three    | 135.8 | 0.22     | 0.22     | 1.03            |
| $\lambda 225T850$ | 5625                | 225       | 850 | Mode three    | 111.1 | 0.18     | 0.18     | 1.04            |
| $\lambda 250T850$ | 6250                | 250       | 850 | Mode three    | 91.2  | 0.15     | 0.15     | 1.04            |

The ultimate strengths obtained from the parametric study ( $F_m$ ) are compared with the values calculated by the proposed formulae ( $F_u$ ) for I-section steel short columns after reaching a temperature, as shown in Table 7. A summary of the experimental and calculated ultimate strength of I-section steel short columns after elevated temperature is presented in Table 8.

A good agreement was obtained with the average values of  $F_m$  to  $F_u$  ratio of 0.987 and the corresponding Coefficient of Variance (COV) of 0.009. Because the average value of  $F_m/F_u$  is 0.987, the calculated strength using Eq. (1) is accurate compared with the experimental results.

When the mean value of  $F_m/F_u$  is 0.987, the max value 1.170, the min value 0.860, and the COV value 0.009. The data shows the high accuracy of Eq. (1) for the prediction of the ultimate strength. It can be seen that the accuracy with which the equation predicted the experimental ultimate strength of I-section steel short columns after elevated temperature is reasonable, and in general the predictions are somewhat accurate.

#### 4.6. Effect of Slenderness Ratio

In order to examine the effects of slenderness ratio ( $\lambda$ ) on the local and global buckling behavior of the columns, another forty FEA models with different slenderness ratios ranging from 25 to 250 were designed and details of these models are listed in Table 9. The section size of all models is the same as model Ix40 $\beta$ 13T20 in chapter 4.1, the temperatures are 20, 550, 700 and 850°C, respec-

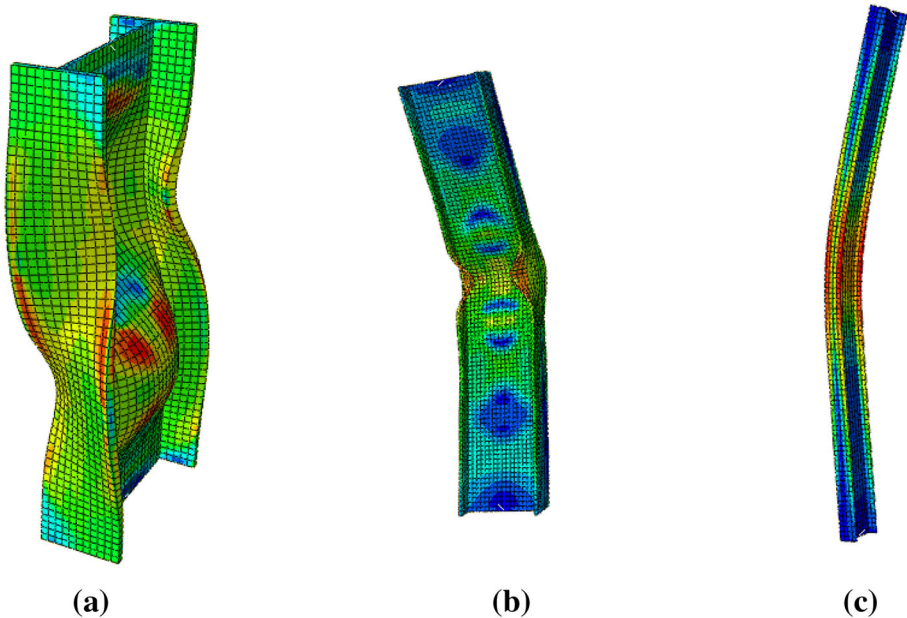


**Figure 14. Failure modes of columns with different slenderness ratio. (a) Mode one, (b) mode two, (c) mode three.**

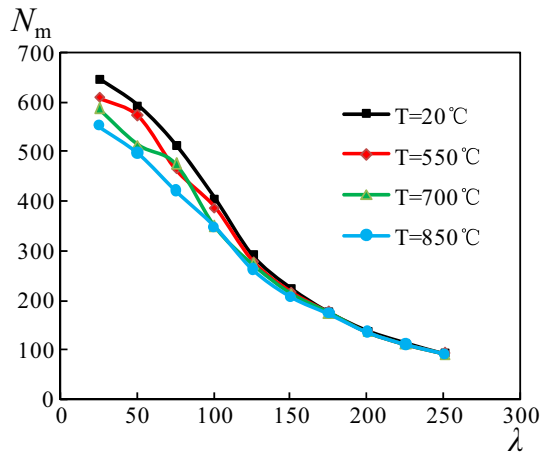


**Figure 15.**  $N_m$  versus  $\lambda$  curves with different T.

tively. It should be noted that the  $\lambda$  is slenderness ratio of the column about the weak axis.

The simulation results show that there are three typical failure modes of the columns with different slenderness ratios, as shown in Fig. 14. For mode one, local buckling occurs at multiple parts of the flange and web. For mode two, local buckling just occurs at mid-height of the columns. Mode three belongs to global buckling. As seen from Table 9, the columns with slenderness ratio of 25 failed with mode one, the columns with slenderness ratio of 50 failed with mode two. When the slenderness ratio of the column was more than 50, the column failed with mode three. It could also be found that elevated temperatures had no evident effects on failure modes of the columns.

Columns with different slenderness ratios failed due to local buckling or global buckling and the load bearing capacities ( $N_m$ ) are listed in Table 9. Relations between  $N_m$  and  $\lambda$  are shown in Fig. 15. From Fig. 15, when  $\lambda$  is less than 150, the load bearing capacity of the columns with the same  $\lambda$  decreases with the increase of the high temperature. When  $\lambda$  is greater than 150 or equal to 150, the load bearing capacity of the columns with the same  $\lambda$  in general does not change with the increase of the high temperature. This can be explained by that the  $\lambda$  is the major factor to determine the load bearing capacity of the columns and the effect of high temperature is not evident when  $\lambda$  is greater than 150 or equal to 150.

The effect of the slenderness ratio on the load bearing capacity of the columns after high temperature exposure can be evaluated by the stability coefficient  $\psi$ , given as follows.

$$\psi = N_m / (f_y \times A_s) \quad (2)$$

The obtained stability coefficient from FEA ( $\psi_m$ ) is listed in Table 9, based on the data, a new predictive formula with considerable precision has been proposed to evaluate the effect of  $\lambda$  on  $\psi$  through regression analysis, as follows.

$$\psi = \frac{1}{2a^2\lambda^2} \left[ 0.965 + 0.3a\lambda + a^2\lambda^2 - \sqrt{(0.965 + 0.3a\lambda + a^2\lambda^2)^2 - 4a^2\lambda^2} \right] \quad (3)$$

where “a” is the temperature effect coefficient and:

$$a = -1.51 \times 10^{-9} \left( \frac{T}{T_0} - 20 \right)^2 + 1.65 \times 10^{-7} \left( \frac{T}{T_0} - 20 \right) + 0.010756 \quad (4)$$

The stability coefficient calculated from the formula ( $\psi_u$ ) is listed in Table 9. What's more,  $\psi_m$  is compared with  $\psi_u$  and the mean value of  $\psi_m/\psi_u$  is 0.99, max value 1.04, min value 0.91, and variance value 0.0019, which prove that the formula can well predict the stability coefficient of the columns with different slenderness ratios after high temperatures exposure.

## 5. Conclusions

This paper presents the experimental results and parametric analysis of I-section steel columns after reaching a high temperature. High temperature duration has limited influence on the ultimate strength of the I-section steel short columns. The residual strength of the I-section steel short columns decreases with the increase of the high temperature exposure, and the higher the specimen temperature is, the faster the ultimate strength declines. Both elevated specimen temperature and its duration have little influence on the initial stiffness, ductility coefficient and yield load to ultimate load ratio of I-section steel short columns, but the yield load decreases with the increase of the maximum specimen temperature. A formula for the ultimate strength of I-section steel short columns after high temperature treatment was proposed on the parameters of high temperature, height-to-thickness ratio of web and width-to-thickness ratio of flange. Parametric observations also infer that the failure modes of the columns are related to the slenderness ratio. When the slenderness ratio of the column was no more than 50, the column failed due to local buckling. When the slenderness ratio of the column was more than 50, the column failed due to global buckling. In addition, the effect of slenderness ratio on the stability coefficient of the columns after reaching a different elevated temperature is quite different. At last, based on the FEA, a new formula has been proposed to predict the stability coefficient of the columns after reaching elevated temperature.

## Acknowledgements

This research work was supported by the National Natural Science Foundation of China (Nos. 51478047 and 51778066) and Hubei Province Outstanding Youth Science Foundation of China (No. 2017CFA070).

## References

1. Tondini N, Hoang VL, Démonceau JF, Franssen JM (2013) Experimental and numerical investigation of high-strength steel circular columns subjected to fire. *J Constr Steel Res* 80:57–81
2. Kervalishvili A, Talvik I (2014) Alternative approach to buckling of square hollow section steel columns in fire. *J Constr Steel Res* 96:140–150
3. Yang KC, Yang FC (2015) Fire performance of restrained welded steel box columns. *J Constr Steel Res* 107:173–181
4. Fan SG, Ding XF, Sun WJ, Zhang LY, Liu MJ (2016) Experimental investigation on fire resistance of stainless steel columns with square hollow section. *Thin Walled Struct* 98:196–211
5. Feng M, Wang YC, Davies JM (2003) Structural behaviour of cold-formed thin-walled short steel channel columns at elevated temperatures. Part 1: experiments. *Thin Walled Struct* 41:543–570
6. Cheng SS, Li LY, Kim B (2015) Buckling analysis of partially protected cold-formed steel channel section columns at elevated temperatures. *Fire Saf J* 72:7–15
7. Scullion T, Ali F, Nadjai A (2011) Experimental study on performance of elliptical section steel columns, under hydrocarbon fire. *J Constr Steel Res* 67:986–991
8. Yang KC, Lee HH, Chan O (2006) Performance of steel H columns loaded under uniform temperature. *J Constr Steel Res* 62:262–270
9. Yang KC, Hsu R (2009) Structural behavior of centrally loaded steel columns at elevated temperature. *J Constr Steel Res* 65:2062–2068
10. Ragheb WF (2016) Estimating the local buckling capacity of structural steel I-section columns at elevated temperatures. *Thin Walled Struct* 107:18–27
11. Correia AJPM, Rodrigues JPC (2012) Fire resistance of steel columns with restrained thermal elongation. *Fire Safety J* 50:1–11
12. Lu J, Liu HB, Chen ZH, Liao XW (2016) Experimental investigation into the post-fire mechanical properties of hot-rolled and cold-formed steels. *J Constr Steel Res* 121:291–310
13. Jin M, Zhao JC, Chang J, Zhang DX (2012) Experimental and parametric study on the post-fire behavior of tubular T-joint. *J Constr Steel Res* 70:93–100
14. ISO 834 (1999) Fire-resistance tests—elements of building construction—part 1: general requirements. ISO 834-1, International Organization for Standardization, Geneva
15. Tao Z, Ghannam M, Song TY, Han LH (2016) Experimental and numerical investigation of concrete-filled stainless steel columns exposed to fire. *J Constr Steel Res* 118:120–134
16. Chinese Code (2002) Metallic materials-tensile testing at ambient temperature. GB/T 228-2002, Beijing, China (**in Chinese**)
17. ABAQUS (2006) Standard user's manual, vols 1–3. Version 6.11. Hibbitt, Karlsson and Sorensen, Inc., Version 6.11, USA